

EVT-701 is a novel selective and safe mitochondrial complex 1 inhibitor with potent anti-tumor activity in models of solid cancers

Raquel Luna Yolba¹ | Virgile Visentin¹ | Caroline Hervé¹ | Johanna Chiche² |
Jean-Ehrland Ricci² | Jérôme Méneyrol¹ | Michaël R. Paillasse¹  | Nathalie Alet¹

¹Evotec SE, Curie Campus, Toulouse, France

²C3M, INSERM, Université Côte d'Azur, Equipe labellisée Ligue Contre le Cancer, Nice, France

Correspondence

Michaël R. Paillasse, Evotec SE, Campus Curie, 195 Route d'Espagne, 31036 Toulouse, France.
Email: michael.paillasse@evotec.com

Funding information

This work was supported by the EU's Horizon 2020 Research and Innovation Programme under the Marie Skłodowska-Curie Grant Agreement 766214 (METACAN). JER's lab is funded by La Ligue Contre le Cancer, le Cancéropole PACA, l'Inserm and the Agence Nationale de la Recherche (LABEX SIGNALIFE ANR-11-LABX-0028-01).

Abstract

Targeting the first protein complex of the mitochondrial electron transport chain (MC1) in cancer has become an attractive therapeutic approach in the recent years, given the metabolic vulnerabilities of cancer cells. The anticancer effect exerted by the pleiotropic drug metformin and the associated reduction in hypoxia-inducible factor 1 α (HIF-1 α) levels putatively mediated by MC1 inhibition led to the development of HIF-1 α inhibitors, such as BAY87-2243, with a more specific MC1 targeting. However, the development of BAY87-2243 was stopped early in phase 1 due to dose-independent emesis and thus there is still no clinical proof of concept for the approach. Given the importance of mitochondrial metabolism during cancer progression, there is still a strong therapeutic need to develop specific and safe MC1 inhibitors. We recently reported the synthesis of compounds with a novel chemotype and potent action on HIF-1 α degradation and MC1 inhibition. We describe here the selectivity, safety profile and anti-cancer activity in solid tumors of lead compound EVT-701. In addition, using murine models of lung cancer and of Non-Hodgkin's B cell lymphoma we demonstrated that EVT-701 reduced tumor growth and lymph node invasion when used as a single agent therapy. LKB1 deficiency in lung cancer was identified as a potential indicator of accrued sensitivity to EVT-701, allowing stratification and selection of patients in clinical trials. Altogether these results support further evaluation of EVT-701 alone or in combination in preclinical models and eventually in patients.

KEYWORDS

DLBCL, LKB1, lung cancer, mitochondrial complex 1, Non-Hodgkin's lymphoma, STK11

Abbreviations: AUC, area under curve; DAPI, 4',6-diamidino-2-phenylindole; DLBCL, diffuse large B-cell lymphoma; ETC, electron transport chain; FCCP, Carbonyl cyanide-p-trifluoromethoxy-phenylhydrazone; IC₅₀, half maximal inhibitory concentration; MC1, mitochondrial complex 1; NH, Non-Hodgkin's; OCR, oxygen consumption rate; OD, optic density; OxPhos, oxydative phosphorylation; PEG, polyethylene glycol; TCA, tricarboxylic acid.

Raquel Luna Yolba and Virgile Visentin contributed equally to the work as first authors.

This is an open access article under the terms of the Creative Commons Attribution-NonCommercial-NoDerivs License, which permits use and distribution in any medium, provided the original work is properly cited, the use is non-commercial and no modifications or adaptations are made.

© 2021 The Authors. *Pharmacology Research & Perspectives* published by John Wiley & Sons Ltd, British Pharmacological Society and American Society for Pharmacology and Experimental Therapeutics.

1 | INTRODUCTION

Since 2000, a growing body of evidence has rehabilitated the importance of mitochondrial metabolism in tumor growth, muzzled for long by Warburg effect supremacy. The very aggressive type of Non-Hodgkin's (NH) B-cell lymphoma, that is, diffuse large B-cell lymphoma (DLBCL) was the first tumor entity in which an increase in the expression of mitochondrial-related genes was identified in the so-called oxydative phosphorylation (OxPhos)-DLBCL subset.¹ Two other independent studies unraveled the key role of mitochondrial metabolism in supporting the growth of **KRAS**-driven lung tumors in mouse models.^{2,3} Since then, many studies demonstrated increased mitochondrial metabolism in melanoma, lung and brain tumors compared to normal tissues.⁴⁻⁷

Furthermore, tumors seem to develop from clones with amplified and functional mitochondria^{8,9} while clones with mitochondrial dysfunction cannot undergo tumorigenesis.¹⁰ Recent work suggests that such metabolic reprogramming is a continuous process, allowing dynamic adaptation as tumor requirements change from initiation to metastasis,¹¹ and in response to anti-cancer therapies.¹²

Mitochondrial complex 1 (MC1) is the first and major component of the electron transport chain (ETC), oxidizing **NADH** from the tricarboxylic acid (TCA) cycle (and fatty acid β -oxidation pathway) to initiate the electron and proton transfer necessary for ATP synthesis.^{13,14} It comprises 44 subunits of which 14 are necessary and sufficient for catalytic activity.^{15,16} Given the number of accessory subunits, its roles in metabolism and cell fitness are multiple and difficult to disentangle. Nevertheless, recent studies shed light to the important roles of MC1 in tumorigenesis and tumor adaptation in nutrient- and oxygen-poor surroundings.

First, the electron transport chain is operational in hypoxic environments, even at oxygen levels below 0.5%¹⁷ and it can still contribute to ATP production and tumor cell survival.^{18,19}

Second, another important role of ETC is to support aspartate biosynthesis. Aspartate is a proteogenic amino acid involved in nucleotide (purines and pyrimidines) biosynthesis, and therefore in proliferation. Active ETC also favors aspartate biosynthesis in order to maintain the level of TCA cycle intermediate levels compatible with cell energetic needs. Furthermore, increased expression and activity of MC1 is correlated with resistance to chemotherapy in pancreatic cancer²⁰ and with metastatic potential in colon cancers.²¹ Finally, MC1 is fully functional in moderate hypoxic conditions and so sustainably maintains low levels of oxygen in tumor. This, in turn, restricts damaging ROS levels and stabilizes the transcription factor HIF-1 α .

Consistent with the important role played by MC1 in tumor survival and growth, a handful of approved drugs inhibiting MC1 (among other targets) have shown anticancer effects in clinical studies. Metformin, for instance, improves the survival of patients with breast, colorectal, ovarian, and liver tumors.^{22,23} Mechanistically, metformin prevents stabilization of HIF-1 under hypoxic conditions in hepatocellular carcinoma.²⁴ This reprogramming of HIF1-driven

metabolism eventually prevents mitochondrial-dependent biosynthesis.²⁵

Among more specific compounds developed over the last decades, BAY87-2243 is of special interest as it was identified from a screen for inhibitors of HIF-1 α -mediated gene transcription under hypoxic conditions. This very potent compound was shown to inhibit MC1 and to induce mitochondrial depolarization and ATP depletion.²⁶ It also increased ROS production, leading to activation of AMP-activated protein kinase (**AMPK**) signaling and apoptosis.²⁷ Unfortunately, clinical development of BAY87-2243 was terminated at phase 1 due to massive and dose-independent induction of emesis in patients. IACS-010759 is a potent and selective MC1 inhibitor identified through a medicinal chemistry program building on the structures of HIF-1 α modulators and known to inhibit oxidative phosphorylation. The agent showed some promise in the treatment of brain tumor and leukemia,²⁸ and a recent phase 1 study in 18 patients with advanced solid tumors showed that the compound was well-tolerated, with initial indications of anti-tumor activity.²⁹

Nevertheless, the clinical potential of MC1 inhibition in cancer remains largely unexplored. Given the complex nature of the target and the limited number of specific agents available, the development of new potent and specific MC1 inhibitors based on different chemotypes is highly desirable.

2 | MATERIALS & METHODS

2.1 | Cell lines and reagents

Lewis lung carcinoma tumor cells, LL/2 (CRL-1642TM), Hep3b.1-7 (HB-8064TM), MDA-MB231 (HTB-26TM), H460 (HTB-177TM) and H1299 (CRL-5803TM) cells were purchased from ATCC[®], KARPAS 422 were from ECACC, purchased from Sigma-Aldrich. The NCI-H460-luc2 human lung cancer cell line was kindly provided by Dr Alain Le Pape (Research Director, Scientific Director of Centre For Small Animal Imaging, CIPA of CNRS Orleans Campus, Orléans, France). LL/2 and MDA-MB-231 were grown in DMEM, H460 and H1299 in RPMI-1640 and Hep3b in MEM, each supplemented with 10% Fetal Bovine Serum, 2 mM Glutamax, 1 mM sodium pyruvate and 1 mM MEM NEAA (non-essential amino acids). ATCC-formulated DMEM, MEM-Earle's medium, RPMI1460, PBS, Hepes, sodium pyruvate, MEM NEAA trypsin, Glutamax and L-glutamine were from Gibco, fetal bovine serum (FBS), BSA, rotenone, antimycin A, iodoacetate, Carbonyl cyanide-p-trifluoromethoxy-phenylhydrazone (FCCP), sodium bicarbonate, D-glucose were from Sigma-Aldrich, Penicillin and streptomycin from Life Technologies, PBS-buffered formalin from Fisher Scientific, mouse standard diet from SAFE, Rompun[®] 2% from Bayer Health Care, Imalgene[®] 1000 from Merial, sodium pentobarbital from Ceva, Isoflurane[®] from Axience, NaCl 0.9% from Aguettant, Hexomedine[®] from Sanofi Aventis, Matrigel[®] from BD Biosciences, D-Luciferine salt from Molecular Probes, PEG200 from Alfa Aesar and Solutol[®] HS15 from BASF.

Mouse primary E μ -Myc cells (murine malignant B-cells) obtained from B-cell lymphomas of independent C57BL/6 E μ -Myc transgenic mice (line hosted at C3M), were isolated as described previously,³⁰ maintained in DMEM supplemented with 10% FBS, 2-mercaptoethanol (50 μ M), L-asparagin (0.37 mM) and HEPES (pH 7.4, 10 mM) and previously characterized as OxPhos or Glycolytic.³¹

Anti-human Ki-67 (Rabbit IgG) was obtained from Abcam (all used 1/200X), anti-human carbonic anhydrase IX (Goat IgG) from R&D System (used 1/100X), anti-human Caspase-3 (Rabbit IgG) from Cell Signaling Technology (used 1/500X), anti-mouse CD31 (Rat IgG) from Biolegend (all used 1/500X); Anti-rabbit, anti-rat HQ, anti-goat HQ and anti-HQ-HRP, Ultra Map DAB kit, ChromoMap DAB Kit, Omnimap anti-Rb HRP and hematoxylin were obtained from DISCOVERY, Roche Diagnostics (all used 1/500X).

2.2 | *In vitro* inhibition of Complex I

MitoTox™ Complex I OxPhos Activity Assay Kit (ab109903), designed for testing the direct inhibitory effect of compounds on Complex I, was used according to the supplier's instructions. The assay uses Complex I purified from bovine heart, immunocaptured by specific antibodies on the plate. Complex I activity is observed as a decrease in absorbance at OD 340 nm, which denotes the oxidation of NADH by mitochondrial complex I.

2.3 | Mitochondria respiration profiling

Twenty thousand cells/well were seeded in a VP3-PS cell culture microplate adapted to an XF96 analyzer (Seahorse Bioscience), and allow to adhere overnight. Growth medium was exchanged with pre-warmed assay medium (XF base medium supplemented with 25 mM glucose, 2 mM glutamine and 1 mM sodium pyruvate; pH 7.4) and incubated at 37°C for 1 h without CO₂ to allow pre-equilibration in assay medium. Pre-warmed oligomycin, FCCP and rotenone plus antimycin A were loaded into injection ports A, B, and C of the sensor cartridge, respectively, to give final concentrations of 1 μ g/ml oligomycin, 1 μ M FCCP, 1 μ M rotenone & 1 μ M antimycin A. For assessment, the compound was loaded into the injector port A and oligomycin, FCCP and rotenone plus antimycin A into the ports B, C, and D, respectively. The cartridge was calibrated by the XF96 analyzer, and the assay was performed with the following parameters: 4 min mix, 3 min measure. Oxygen consumption rate (OCR) was detected under basal conditions followed by the sequential addition of 10X solutions containing the different doses of the compound to evaluate, followed by three sequential additions of FCCP at a final concentration of 0.3, 1, and 3 μ M to uncouple mitochondria. Control injections were with medium. Data are presented as the fold of the OCR of the given dose of compound to vehicle. Figure S4 shows a representative OCR curve of a Seahorse experiment with H460 cell line.

2.4 | Quantification of total and mitochondrial ATP content

Total and mitochondrial ATP content was measured by using Cell Titer Glo assay (Promega) according to the manufacturer's protocol. Iodoacetate was used as specific glycolysis inhibitor to define the origin of ATP and to isolate the effect of compounds on mitochondrial function, since it inhibits glycolysis by the alkylation of the essential cysteine residue in the active center of GAPDH, which results in impaired enzyme activity.^{32,33} Thus, the compound effect is measured on the total ATP content and on the mitochondrial ATP content (measured in the presence of 100 μ M iodoacetate). Cells were seeded at 8000 cells/well in 80 μ l of complete medium (96-well plates) and incubated at 37°C (95% air; 5% CO₂) for 18 h. Compounds were added (10 μ l of a 10X solution in culture media to obtain half-log dose-response with final concentrations in 10 nM to 10 μ M range) to pairs of plates and the cells were incubated for 1 h in the presence or not of iodoacetate (addition of 10 μ l of culture media or of 10 μ l of a 10X iodoacetate solution). At the end of the incubation time, the ATP content was measured by using the Cell Titer Glo according to the manufacturer's protocols. The luminescence signal was recorded with a microplate reader (2103 EnVision™ Multilabel Plate Readers—PerkinElmer). Raw data (Relative Luminescence Units) were analyzed using Microsoft Excel 2016 software; values represent mean \pm standard deviation. Mitochondrial ATP is determined with iodoacetate, global ATP without.

2.5 | Proliferation & apoptosis measurement assays

Cells were seeded at 5000 cells/well in 80 μ l/well in culture media using 96-well plates. After overnight incubation at 37°C (95% air, 5% CO₂), 10 μ l of 10X solutions of the compound were added to the appropriate wells (in culture media to obtain dose-response with final concentrations in 10 nM to 10 μ M range). For apoptosis determination, an additional 10 μ l of Caspase-3/7 green reagent (Essen Bioscience, Catalog # 4440) diluted at 1/200 in corresponding media was added to the wells. Caspase-3/7 green reagent only emits fluorescence when it is cleaved by activated Caspase-3/7, resulting in the release of the DNA dye and green fluorescent staining of nuclear DNA, which allows the monitoring of the kinetic activation of caspase-3/7. Plates were immediately placed in Incucyte live-cell, time-lapse imaging system allowing the visualization and quantification of cell proliferation and apoptosis over time (Incucyte Zoom, Essen Bioscience Sartorius) for image acquisition. Two images were acquired under phase and green fluorescence (400 ms acquisition time by default) every 3 h, at 10X magnification for 96 h for the first experiment and then for 72 h for the three subsequent experiments. Assessment of cell confluence was based on phase images and apoptosis assessment was based on green fluorescence images. The Incucyte software (Incucyte ZOOM Version 2018A) was used to generate the kinetic graphs from the proliferation and apoptosis data. Changes in % of cell confluence for proliferation and of

fluorescent counts for apoptosis were represented as % or fold to vehicle both for apoptosis and proliferation. **Proliferation:** Although there were changes in cell morphology as cells proliferate and confluence increases, we decided to use confluence as the measure of cell proliferation to assess the effect of the small molecules on cell proliferation. Cell proliferation was monitored by analyzing the occupied area (% confluence) of cell images over time. **Apoptosis:** Apoptosis was monitored using the caspase-3/7 green apoptosis assay reagent. When added to the tissue culture medium, this inert, non-fluorescent reagent crosses the cell membrane where it is cleaved by activated caspase-3/7 that releases the DNA dye and that results green fluorescent staining of nuclear DNA. Apoptosis was determined by counting the number of fluorescence objects in each well and was expressed as cells/mm². The fluorescence threshold was set to 1 GCU, meaning that each object above this threshold was detected in the image.

2.6 | *In vitro* cell death assay in the Eμ-Myc model

Eμ-Myc cells (2×10^5) were seeded in 96-well plates in the presence or absence of EVT-701 (at indicated doses) for 24 h. Cells were then labeled with DAPI (Molecular Probes; 0.5 μg/ml) and analyzed immediately by flow cytometry using a MACSQuant Analyzer (Miltenyi Biotec). Cell death induction represents the percentage of DAPI positive cells in EVT-701-treated conditions divided by the percentage of DAPI positive cells in control (DMSO) conditions.

2.7 | Animals

Female C57BL/6, male Balb/CJ-Nude, and female CB17 SCID mice were purchased from Charles River Laboratories. The nycthemeral cycle in the housing room is 12/12-h light/dark, the room temperature was at $22 \pm 2^\circ\text{C}$ with $55 \pm 10\%$ of relative humidity. The mice were fed *ad libitum* with a standard diet and filtered tap water. The laboratory animal care program and the animal facility have been fully accredited by AAALAC organization. All the experimental procedures were approved by the local ethics committee of the company and were registered at the French Ministry of Higher Education and Research.

2.8 | Orthotopic LL/2 lung tumor model

Cell implantation procedure: LL/2 cells were grown in a 5% CO₂ humidified atmosphere (90%) at 37°C, in DMEM medium supplemented with 3% FBS and L-glutamine 2 mM. The cells were trypsinized, washed with PBS and adjusted to a concentration of 50 000 cells/ml in Matrigel and PBS/BSA 0.1% (1:4; v:v). The cell suspension was kept at 4°C until inoculation into mice. 7-week-old female C57/Bl6 mice were anesthetized with a mixture of Rompun®2% (20 mg/kg) and Imalgene®1000 (100 mg/kg) in NaCl 0.9% at 10 ml/kg

by intraperitoneal injection. A small skin incision to the left chest wall (<1 cm) was made at about 5 mm tail side from the scapula. Subcutaneous fat and muscles were separated from costal bones. LL/2 cells (1000 cells suspended in 20 μl) were directly injected through the intercostal space into the left lung. The area of injection was cleaned with Hexomedine®. The incision was closed with a surgical skin clip. At study termination, the mice were euthanized by barbiturate overdose (sodium Pentobarbital). The ribcage was opened and the left lung and the mediastinal lymph nodes were removed. Lung tumors were measured using an electronic caliper in order to determine the tumor volume (V) according to the formula: $V = l^2 \times L \times 0.52$ (l = width and L = length) and the mediastinal lymph nodes were weighed. Statistical analysis was performed using *t*-test for tumor volumes and lymph node weights. **Treatment schedules:** Mice were allocated to experimental groups based on body weight at the initiation of the treatment. At the end of the studies, mice without tumors were excluded from the statistical analysis. LL/2 tumor-bearing mice were dosed orally with either placebo (vehicle) or with EVT-701, 14 mice were allocated to each group. Mice received 14 (from D10 to D23 post cell inoculation) or 4 (from D19 to D22 post cell inoculation) consecutive single oral daily administrations with 10 and 30 mg/kg of compound according to the study design. EVT-701 was prepared daily as 1 and 3 mg/ml solutions in PEG200/Solutol®HS15/water (30%/5%/65%) and administered to mice at 10 ml/kg by oral gavage.

2.9 | Orthotopic H460 lung tumor model

Cell implantation procedure: H460-Luc2 cells were grown in a 5% CO₂ humidified atmosphere (90%) at 37°C, in RPMI1640 medium supplemented with 10% FBS, D-Glucose (4.5 g/L), Glutamax 2 mM, Sodium pyruvate 1X, sodium bicarbonate (2 mM) and Hepes buffer (10 mM). The cells were trypsinized, washed with PBS and adjusted to a concentration of 20 million cells per ml in PBS. The cell suspension was kept at 4°C until inoculation into mice. Seven-week-old male Balb/c Nude mice were anesthetized with a mixture of Rompun®2% (20 mg/kg) and Imalgene®1000 (100 mg/kg) in NaCl 0.9% at 10 ml/kg by intraperitoneal injection, and subsequently placed on an angular board in order to visualize the glottis using a light source, an otoscope, and a modified spatula. The mice were inoculated with 25 μL of cell suspension using a S/L First PICC 26G (1.9F) blunt-end silicon catheter inserted into the bronchus through the mouth. Tumor progression was followed by bioluminescence imaging (BLI) at D7, D14 and D21 post cell inoculation. Animals were anesthetized with isoflurane® vaporized to 2.5% in O₂/Air = 1 L/min. D-luciferin was applied by intraperitoneal injection (2 mg/mouse in 200 μl). Bioluminescence was measured 12 min after using an IVIS spectrum imager (PerkinElmer). At termination, the ribcage was opened, the lungs were removed and tumors were measured as described for the LL/2 model. Statistical analysis was performed using *t*-test for tumor volumes and weights, and two-way repeated measures ANOVA for bioluminescence. **Treatment**

schedule: Mice were allocated to experimental groups based on bioluminescent signal of the tumors at the initiation of the treatment (D7 post cell inoculation). H460-Luc2 tumor-bearing mice received 15 consecutive single daily oral administrations with 30 mg/kg of compound according to the study design. EVT-701 was prepared daily as 3 mg/ml solutions in PEG200/Solutol®HS15/water (30%/5%/65%) and administered to mice at 10 ml/kg by oral gavage ($n = 9$ mice/group). Control mice received PEG200/Solutol HS15/water (30%/5%/65%) as vehicle ($n = 9$ mice/group).

2.10 | EVT-701 level assessment in plasma and tumor of LL/2 tumor-bearing mice

Blood samples were collected from the abdominal aorta and transferred into glass tubes containing lithium heparin. Immediately after sampling, the individual blood samples were centrifuged at 8000 g for 10 min at 4°C. Plasma samples were frozen at -20°C until analysis. LL/2 tumors were collected, pooled (3 mice per sampling time), weighed, and frozen at -20°C until analysis. One gram of tissue being mixed with 2 ml of water for homogenization. After the addition of the precipitant solution (CH₃CN), EVT-701 was quantified by LC-MS/MS. **LC-MS/MS conditions:** Analysis performed on Thermo Accela LC with HTC CTC-Pal autosampler. Column: Luna C18 Phenomenex (50 × 2.1 mm) 3 μm; Elution conditions: Eluent A = H₂O + ammonium acetate 0.015% (w/v) + formic acid 0.2% (v/v); Eluent B = MeOH 20% (v/v) + ammonium acetate 0.015% (w/v) + formic acid 0.2% (v/v), CH₃CN to 100% volume. T = 25°C. Gradient: 10% B for 0.5 min, to 90% in 1.5 min, 1 min 90% B, back to 10% in 0.5 min and 1.5 min 10% B; Flow rate = 0.7 ml/min; injection 5 μl, retention time 2.3 min. Analysis conditions: Thermo TSQ Quantum Ultra 4 mass spectrometer, ES+, cone tension 46 V, capillary T = 350°C, vaporizer T = 350°C. *m/z* transition 630.03 ≥ 270.05; Software: Excalibur version 2.1.0. **Preparation of quality control and calibration samples:** Quality Control samples and Calibration Samples were prepared daily by spiking mouse plasma with working solutions prepared from independent EVT-701 weightings. The calibration curve was calculated from calibration levels at 1 ($n = 3$), 2.5, 5, 10, 25, 50, 100, 200 ($n = 3$), 500, 1000, and 2000 ($n = 3$) ng/ml. The concentrations for Quality Controls were 5, 50, 150, 450, and 1500 ng/ml. Analysis used quadratic regressions (not forced through the origin) weighted by 1/x. The limit of quantification (LOQ) was estimated to 2.5 ng/ml for the plasma and 10 ng/ml for the LL/2 tumors. The pharmacokinetic parameters were calculated from the arithmetic mean of the plasma concentrations or the LL/2 tumor concentrations using the program WinNonLin 5.2, non-compartmental model 200.

2.11 | B-cell lymphoma *in vivo* studies

Lymphoma transfer of isolated Eμ-Myc clones was realized into syngeneic, non-transgenic, 6-week-old C57BL/6J Ola Hsd

female (Envigo) by tail vein injection of 1×10^5 viable Eμ-Myc cells per recipient mouse (in 150 μl of sterile PBS). As the inguinal lymph nodes became “palpable” (six days after cell injection), the animals were treated daily with 30 mg/kg of EVT-701 (oral; 10 ml/kg) or vehicle. EVT-701 powder was dissolved daily in PEG200/Solutol HS15/water (30%/5%/65%). Control mice received PEG200/Solutol HS15/water (30%/5%/65%) as vehicle ($n = 10$ mice/group). Food and water were given ad libitum. Mice weight and palpation of the inguinal lymph nodes were determined every two or three days. Eμ-Myc lymphoma-bearing animals were sacrificed as soon as they presented several signs of illness. Upon sacrifice, all lymph node tumors and spleens were collected and weighted. Two hours after the last EVT-701 administration, mice were anesthetized with pentobarbital (75 mg/kg i.p). 500 μl of blood was collected for plasma isolation (lithium heparinate-coated tubes [BDMicrotainer®]) were centrifuged at 6000 g for 1.5 min at room temperature, according to the manufacturer's instructions) before mice sacrifice. Upon sacrifice, all lymph node tumors and spleens are immediately collected and weighted.

Mice were maintained in specific pathogen-free conditions and experimental procedures were approved by the Institutional Animal Care and Use Committee and by the regional ethics committee (PEA232 from Comité Institutionnel d’Ethique Pour l’Animal de Laboratoire – AZUR).

2.12 | Gene set enrichment analysis

The publicly accessible transcriptomic data from The Cancer Genome Atlas Lung Adenocarcinoma (TCGA-LUAD) and The Cancer Genome Atlas Lung Squamous Cell Carcinoma (TCGA-LUSC) cohorts were used in this study. GSEA was performed using DESEQ2 and fGSEA R packages. Gene sets were downloaded from GSEA website (<https://www.gsea-msigdb.org/gsea/msigdb/>). Volcano plots and enrichment maps were used for the visualization of the GSEA results. For each gene signature, its Normalized Enrichment Score (NES) and False discovery rate (FDR) considering the *p*-adjusted values (*padj*) were evaluated. NES with FDR <0.05 were considered significant.

2.13 | Statistical analysis

Data are expressed as mean (±SD). Otherwise notified, these are means of three independent experiments, with three replicates per experiment. Differences in calculated means between groups were assessed by two-sided Student *t*-tests. For time-to-event variables, the survival functions were estimated with Kaplan-Meier method and compared with log-rank tests. All statistical analyses were done with Prism software. A *p*-value of less than .05 was considered to indicate statistical significance (**p* < .05, ***p* < .01 and ****p* < .001).

dose-dependent effect of EVT-701 on isolated MC1 complex. EVT-701 reduces NADH abundance with an IC_{50} of 300 nM (Figure 1B). To assess the effect of EVT-701 on the respiration of isolated mitochondria, we performed polarographic studies. EVT-701 dose-dependently inhibits NADH oxidation and phosphorylation of ADP into ATP by 80% at 7.5 μ M (Figure 1C). Next, we selected three different cancer cell lines in which metformin was reported to dose-dependently inhibit mitochondrial function and/or ATP production, namely MD-MB-231,³⁸ Hep3B³⁹ and U87⁴⁰ cells. While MDA-MB-231 and U87 cells mainly produce ATP through glycolysis, Hep3B cells produce only 40% of their total ATP through glycolysis (Figure 1C). Nevertheless, EVT-701 inhibited mitochondrial ATP production at nanomolar concentrations in all cell lines (IC_{50} of 52 ± 18 , 81 ± 12 and 74 ± 38 nM for MD-MB-231, Hep3B, and U87, respectively), regardless of their basal metabolism (Figure 1E). Selectivity of EVT-701 was assessed on live Jurkat cells through a kinase selectivity panel from DiscoverX[®], based on the KiNativ[®] In situ kinase profiling assay.⁴¹ Among the 198 kinases evaluated in the panel, no kinase activity was inhibited by more than 30% and only MLK2 activity was increased by more than 30% by 10 μ M EVT-701 (Figure 1F), as determined by assessing the phosphorylation state of specific target peptides for each kinase. To evaluate the developability of EVT-701, we performed further safety and ADME assays. The first of these was the *in vitro* safety screen from Cerep[®], based on the ability of EVT-701 at 10 μ M to compete for the binding of reference ligands to 300 receptors. Only one receptor (A2AR) showed ligand binding decreased by more than 50%, while increase greater than 50% was only seen with CCK1R and CCK2R (Figure S1A). While evaluating EVT-701 in mouse acute myeloid leukemia, we verified that its inhibitory effect on respiration was rescued by succinate (Luna Yolba, *in revision*). Pharmacokinetic parameters of EVT-701 were determined using C57BL/6J mice following intravenous administration of EVT-701 (3 mg/kg) and escalating oral dosing (10, 30, and 75 mg/kg). Blood was sampled over 48 h to obtain key PK variables (C_{max} , t_{max} , AUC, $t_{1/2}$, t_{last} , clearance, volume of distribution, and bioavailability). The plasma concentrations of EVT-701 over the 48 h time-course are shown in Figure S1B and PK parameters summarized in Figure S1C. Key features of the data were the extended $t_{1/2}$ (4.1 h), good bioavailability (64%) and the observation that dose-proportionality was conserved from 10 to 75 mg/kg. These measures are all supportive of further *in vivo* evaluation using oral route and a QD regimen. Tissue distribution was measured in the same strain of mice after single oral administration of 30 mg/kg, this showed accumulation of EVT-701 (compared to plasma) in all tissues except the brain (Figure S1D), making EVT-701 potentially suitable for the treatment of several cancer types to the exception of CNS tumors. Specifically, tissue versus plasma AUC ratio was 5.9 for liver, 4.5 for kidney and pancreas, 4.2 for heart, 2.3 for lung, and 0.25 for brain. In order to investigate the mechanism underlying this widespread distribution and address potential efflux issues, we evaluated the interaction of EVT-701 with key transporters from ATP-binding cassette (ABC) and solute carrier (SLC) families, expressed either in CHO, HEK, or MDCKII cells. The compound inhibited OATP1B1,

OATP1B3 and BCRP-mediated transport with respective IC_{50} s of 1.1 ± 0.1 , 2.4 ± 0.2 , and 4.1 ± 2.7 μ M, whereas IC_{50} s for OAT1, OCT1, and MRP2 were higher than 30 μ M and P-gp transport was not affected (Figure S1E). Collectively, these results are consistent with a massive uptake of EVT-701 in the liver, kidney, and intestine but could also provide a potent mechanism of elimination via kidney excretion. Finally, to examine to what extent safety issues reported for BAY87-2243 could be relevant for EVT-701, we tested the compounds in a ferret model of emesis at Porsolt. Ferrets were exposed to increasing doses of both compounds. For BAY87-2243, we chose as target concentration C_{max} reported in first patients treated with recommended starting dose in clinical phase 1; for EVT-701, we chose as target dose the estimated C_{max} obtained at steady state in patients to be treated with predicted Dose-to-Man. This was assessed by allometric methods, using rat & mouse PK parameters and considering *in vitro* proliferation IC_{50} as the minimum concentration at steady state. Dose escalation was eventually limited by toxicity for BAY87-2243 and by solubility for EVT-701. In conclusion, BAY87-2243 induced retches and vomits from half of the first patient C_{max} , whereas in similar conditions EVT-701 didn't, showing its safer profile.

3.2 | EVT-701 reduces mitochondrial ATP production and the development of OxPhos but not of glycolytic NH B-cell lymphomas

Targeting mitochondrial metabolism of OxPhos-dependent NH B-cell lymphomas demonstrated a high potential as anti-cancer strategy.⁴² Accordingly, EVT-701 treatment dose-dependently inhibited mitochondrial ATP production with IC_{50} of 393 ± 83 nM (Figure 2A) and proliferation with IC_{50} of 188 ± 50 nM (Figure 2B) in the human OxPhos-DLBCL cell line KARPAS 422.⁴³ This was accompanied by an increased glucose consumption and lactate release (Figure 2C).

We previously established that murine primary Myc-driven B-cell lymphomas arising from the E μ -Myc mice model⁴⁴ display distinct metabolic profiles and energetic status.³¹ Moreover, we demonstrated that E μ -Myc lymphomas relying on OxPhos for energy production are sensitive to specific inhibitors of mitochondrial metabolism such as phenformin, in *in vitro* and *in vivo* settings while glycolytic counterparts were resistant.³¹ *In vitro*, using five independent OxPhos-E μ -Myc and five independent glycolytic-E μ -Myc lymphoma cells, we show that OxPhos-E μ -Myc cells are more sensitive to 10 μ M EVT-701 than glycolytic-E μ -Myc cells (Figure 2D,E). To further test the specific anti-tumor efficacy of EVT-701 on B-cell lymphoma development, one OxPhos-E μ -Myc (clone 506) and one glycolytic-E μ -Myc (clone 504) lymphoma were transferred to syngeneic wild-type immunocompetent C57BL/6 mice. Six days after cell injection, mice were daily dosed with 30 mg/kg of EVT-701 (or Vehicle) given orally. EVT-701 treatment had no effect on the overall survival of glycolytic-E μ -Myc-bearing mice (Figure 2F) nor on the progression-free survival (data not shown). Accordingly, the weight of lymphomas from Vehicle or EVT-701-treated glycolytic-E μ -Myc-bearing

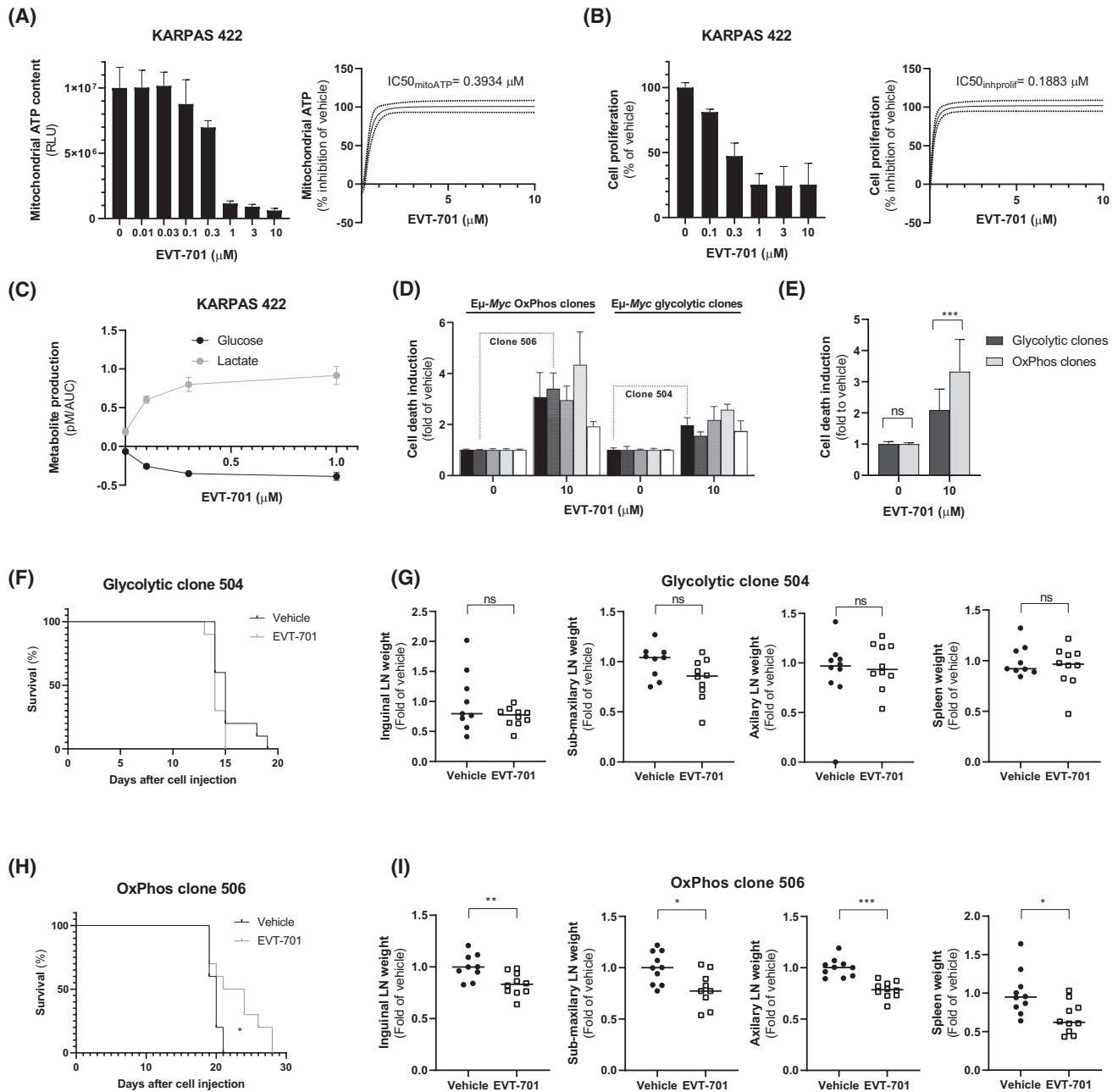


FIGURE 2 EVT-701 is active *in vitro* and *in vivo* in NH B-cell lymphoma models. (A) Dose dependent inhibition of mitochondrial ATP by EVT-701 in KARPAS 422 cell line, with an IC_{50} of 394 nM. (B) Dose-dependent inhibition of KARPAS 422 proliferation by EVT-701, with an IC_{50} of 188 nM. (C) Dose-dependent modulation of glucose consumption and lactate secretion in KARPAS 422 by EVT-701. The compound induces a significant increase in glucose consumption and lactate secretion. (D) OxPhos-E μ -Myc (lymphomas 249, 506, 549, 585, 508) and Glycolytic-E μ -Myc (lymphomas 504, 251, 115, 136, 337) cells were seeded in the presence (EVT-701) or absence (DMSO) of indicated concentration of EVT-701 for 24 h. Cell death was determined by DAPI staining and analyzed by FACS. Cell death induction represents the percentage of DAPI positive cells in EVT-701-treated conditions divided by the percentage of DAPI positive cells in control (DMSO) condition. (E) Summary as the mean of 4 independent experiments ($n = 5$ independent clones per group) is presented. (F) Kaplan–Meier curve of overall survival of syngeneic C57BL/6 mice intravenously injected with glycolytic-E μ -Myc lymphoma cells and treated with 30 mg/kg (p.o, QD) or vehicle until ethical endpoint was achieved. 10 mice per group were used. (G) Inguinal, submaxillary, axillary lymphomas and spleen weights upon sacrifice of glycolytic-E μ -Myc-bearing mice. (H) Kaplan–Meier curves of overall survival of syngeneic C57BL/6 mice intravenously injected with OxPhos-E μ -Myc lymphoma cells and treated with 30 mg/kg (p.o, QD) or vehicle until ethical endpoint was achieved. Ten mice per group were used. (I) Inguinal, submaxillary, axillary lymphomas, and spleen weights upon sacrifice of OxPhos-E μ -Myc-bearing mice. *In vivo* data represent an average of two independent experiments

mice is similar (Figure 2G). However, EVT-701 treatment significantly reduced the progression of OxPhos-E μ -Myc-lymphomas as shown by a significant increase in the overall survival (Figure 2H)

and in the progression-free survival (not shown) of those mice. Lymphomas harvested from EVT-701-treated OxPhos-E μ -Myc-bearing mice were significantly smaller than those of Vehicle-treated

OxPhos-E μ -Myc-bearing mice (Figure 2I). Altogether, our results demonstrated that EVT-701 holds potential as anti-cancer treatment in the context of highly aggressive type of NH B-cell lymphomas dependent on mitochondrial metabolism.

3.3 | EVT-701 inhibits OxPhos metabolism and proliferation of non-small cell lung cancer (NSCLC) lines *in vitro* and *in vivo*

A previously published cohort study of over 7000 patients with NSCLC identified that those receiving concomitant metformin treatment had improved outcomes, suggesting that the anti-metabolic drug could influence cancer progression.⁴⁵ We therefore considered that NSCLC was a good candidate for further evaluation of the anti-tumor potential of EVT-701. We used a syngeneic mouse model of NSCLC involving orthotopic injection of LL/2 cells. This cell line was selected as the parent line—Lewis lung carcinoma (LLC)—is reportedly relevant for assessment of both antitumor and anti-metastatic effects.⁴⁶ LL/2 cells poorly rely on glycolysis (18%) to produce ATP (not shown) which suggests an important role of mitochondrial metabolism. *In vitro*, EVT-701 dose-dependently inhibited mitochondrial energetics in LL/2 cells, as shown by a reduction in ATP production with an IC₅₀ of 512 ± 109 nM (Figure 3A) and proliferation with an apparent IC₅₀ of 295 ± 52 nM (Figure 3B). *In vivo*, when used as a single agent, EVT-701 reduced tumor growth of LL/2 cells injected orthotopically into C57BL/6 mice left lung. Both doses of 10 and 30 mg/kg of EVT-701 significantly inhibited tumor growth (−57% and −69% volume respectively). PK performed during first day of treatment showed accumulation of EVT-701 in tumor compared to plasma, tumor/plasma AUC ratios being 2.9 and 2.5 for 10 and 30 mg/kg, respectively (Figure 3C,D). We then evaluated the influence of time to treatment onset on metastasis in addition to tumor growth. LL/2 orthotopic tumors were treated with EVT-701 (30 mg/kg) either for 14 days from D10 (early onset) or for 4 days from D19 (late onset). The effect on primary tumor growth was similar (66% and 65% decrease of tumor volume, respectively) whereas early onset gave an enhanced benefit in terms of lymph node invasion (64% vs. 34% decrease of lymph node weight—Figure 3E,F).

Among NSCLC tumors, those carrying **LKB1** mutations or with LKB1 downregulation (~20% of all NSCLC) have been reported as highly sensitive to metformin and phenformin.⁴⁷ We therefore used the NCI-H460 (hereafter H460) cell line as a model of LKB1-deficient NSCLC. *In vitro*, EVT-701 not only showed dose-dependent inhibition of mitochondrial ATP production (with an IC₅₀ of 203 ± 53 nM; Figure 3G); OCR (Figure 3H); and proliferation of H460 cells (with apparent IC₅₀ of 68 ± 27 nM; Figure 3I), but also induced apoptosis with an IC₅₀ of 96 ± 28 nM (Figure 3J) whereas no significant cell death was induced in LL/2 even at 10 μ M.

We next assessed the activity of the BAY87-2243 in same model under the same conditions and identified a clear discrepancy between the effects of EVT-701 and BAY87-2243. While mitochondrial ATP production, proliferation and apoptosis were significantly

inhibited by BAY87-2243 at doses less than or equal to 1 nM, we only detected an effect on OCR at doses above 100 nM (Figure S2A–C). These findings support the hypothesis that the undesirable emetic side-effects of BAY-2243 are due to off-target effect(s) rather than inhibition of oxidative metabolism.

To evaluate *in vivo* effect of EVT-701 in LKB1-deficient NSCLC, luciferase-expressing NCI-H460 cells, hereafter H460-luc2,⁴⁸ were orthotopically injected into Balb/CJ-Nude mice and treated daily for 14 days with EVT-701 30 mg/kg starting from D7 (Figure S3A). Mice were randomized based on bioluminescence imaging (BLI—Figure S3B). Unfortunately, BLI could not be used to monitor tumor growth until the end of the experiment as signal was partially lost after D14 (data not shown), presumably due to large the hypoxic and apoptotic zones appearing in vehicle-treated group tumors (Figure S4C shows CAIX, Ki67 and Caspase 3 staining in those tumors). Nevertheless, tumors could be harvested at D21, allowing us to determine that EVT-701 significantly decreased tumor volume by 60% and weight by 57% (Figure S3D,E).

3.4 | LKB1 status is an important factor driving sensitivity of NSCLC cells to EVT-701

Metformin and Phenformin are reportedly highly active on LKB1-mutant NSCLC models. This is potentially linked to the inability of LKB1-mutated cells to modulate AMPK signaling and adapt to metabolic stress. According to this view, LKB1 tumor cells continue uncontrolled growth despite the inhibition of OxPhos, leading to rapid depletion of energy resources and eventually triggering apoptosis.^{6,47} To evaluate LKB1 proficiency/deficiency effect on EVT-701 activity, we established LKB1-overexpressing H460 cell line (H460-LKB1) as compared to wild type H460. Both cell lines were relying more on glycolysis to produce ATP (59% and 75%, respectively—Data not shown). In H460-LKB1, similar to the effect observed with wild type H460, EVT-701 dose-dependently inhibited mitochondrial ATP production with IC₅₀ of 232 nM (Figure 4A); however, we saw no induction of apoptosis even at 10 μ M in the LKB1 proficient cells oppositely to LKB1 deficient cells (Figure 4B). In addition, we could monitor that the phosphorylation cascade downstream of AMPK is activated in EVT-701-treated H460-LKB1 cells, as shown by an increased phosphorylation state of 4E-BP1 on Serine 65, Raptor and Acetyl CoA carboxylase (ACC) within minutes after exposure to EVT-701, whereas parental H460 couldn't (Figure 4C). A growing body of evidence is accumulating of increased TCA cycle activity, mitochondrial membrane potential, and mitochondrial respiration^{49–51} in LKB1-deficient cancer cells to support their proliferation and survival.⁵² Borzi and colleagues proposed that even NSCLC showing low expression of wild-type LKB1 could undergo this metabolic evolution and may accordingly be more sensitive to antimetabolic drugs.⁵³ We therefore interrogated the TCGA database to see if there was evidence to support this metabolic evolution model in larger NSCLC patient cohorts. We addressed lung adenocarcinoma and squamous cell carcinoma cohorts (LUAD and LUSC, respectively) separately. Within each cohort, patients were divided into **LKB1** high and **LKB1** low

sub-cohorts based on median *LKB1* mRNA expression levels. We performed gene set enrichment analysis (GSEA) in *LKB1* low versus *LKB1* high sub-cohorts and observed that mitochondrial metabolism-related

pathways are enriched in *LKB1* low group (Figure 4D,E), in alignment with the conclusions reached by Kaufman and Borzi. Altogether, those results support use of EVT-701 in *LKB1* deficient and *LKB1*-low NSCLC.

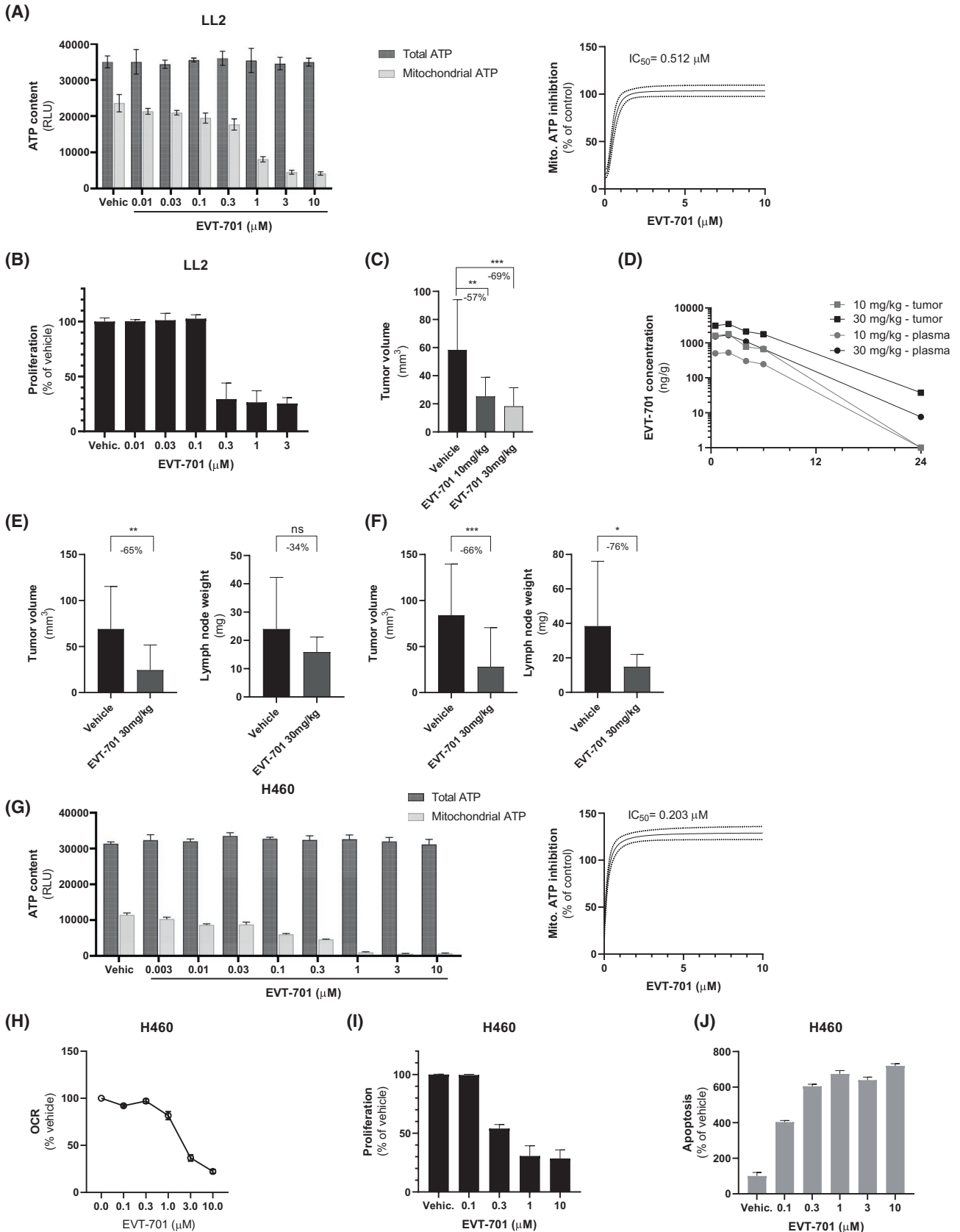


FIGURE 3 *In vitro* and *in vivo* EVT-701 activity in lung cancer. EVT-701 decreases OxPhos and proliferation *in vitro* in several lung cancer cell lines, and shows efficacy *in vivo* in LL/2 orthotopic model. (A) Dose dependent inhibition of mitochondrial ATP in LL/2 by EVT-701, with IC_{50} of 512 nM while in same conditions global ATP remains unchanged whatever the dose of EVT-701. (B) Dose-dependent inhibition of LL/2 proliferation by EVT-701. (C) EVT-701 efficacy in LL/2 *in vivo* orthotopic model. Comparison of efficacy of 10 and 30 mg/kg EVT-701QD dosing for 14 days. Lower dose inhibited tumor growth by 57% while 30 mg/kg inhibited by 69% and the difference between the effects of the two doses was not statistically significant. (D) Evaluation of EVT-701 blood exposure after single administration of 10 or 30 mg/kg. Exposures and exposure ratio (AUC) were consistent with pharmacodynamics studies shown in Figure S1. (E) EVT-701 4-day treatment reduced tumor growth by -65% (right) and lymph node weight by -34% (left). (F) EVT-701 14-day treatment reduced tumor growth by -66% (right) and lymph node weight by -76% (left). (G) Dose-dependent inhibition of mitochondrial ATP in H460 cell line by EVT-701, with IC_{50} of 203 nM. Under the same conditions, global ATP remains unchanged at all doses of EVT-701. (H) Dose-dependent reduction of oxygen consumption in H460 cells by EVT-701 measured by Seahorse. (I) EVT-701 dose-dependent inhibition of proliferation in H460. (J) EVT-701 dose-dependent apoptosis induction in H460 cells. *In vivo* data represent an average of two independent experiments

4 | DISCUSSION

We present here the preclinical characterization of EVT-701, a structurally novel mitochondrial complex 1 inhibitor. The results demonstrate that EVT-701 is a highly potent and selective MC1 inhibitor in a range of biochemical and cell-based assays. Significantly the compound is free of the side effects that interrupted the clinical development of BAY87-2243. While first-in-human trial results with IACS-010759 were reassuring with regard to toxicity, it shares the BAY87-2243 backbone and so uncertainty about its safety remains. EVT-701 is the product of a discovery program aimed at finding HIF-1 α -destabilizers with a new scaffold to circumvent the aforementioned side effects.

Pointing to the therapeutic potential of EVT-701 for solid tumor treatment, proliferation of non-small cell lung cancer (NSCLC) and DLBCL cell lines *in vitro* and tumor growth in syngeneic and xenograft NSCLC and NH B-cell lymphoma models were potently inhibited by EVT-701. Mice bearing NH B-cell lymphoma tumors originating from high OxPhos clones showed prolonged survival after EVT-701 treatment. Functional studies showed that reduction of tumor cell growth was correlated with inhibition of NADH oxidation, oxygen consumption rate and mitochondrial ATP formation, paralleled with an increase in glucose consumption and lactate production, altogether concurring with MC1 inhibition. Using and growth of syngeneic and xenograft NSCLC and NH B-cell lymphoma models we demonstrated that EVT-701 hold potential as anti-cancer agent dedicated to OxPhos-dependent tumors since it prolonged survival of OxPhos-E μ -Myc lymphoma-bearing mice, but not for glycolytic-E μ -Myc-lymphoma-bearing mice.

It became clear over the last decades that despite their glucose addiction, tumors still largely use oxidative phosphorylation to support survival and growth.

Liver kinase B1 (LKB1), also known as serine/threonine kinase (STK11) has been characterized as a tumor suppressor gene. In a cancer setting, LKB1 suppressed malignant cell transformation and drastically decreased tumor progression.⁵⁴ Mutation in LKB1 has been identified as a possible causative factor for Peutz-Jeghers syndrome,⁵⁵ a genetic disorder where patients show an increased risk of cancer.⁵⁶ This has been evidenced for pancreatic and non-small cell lung cancers, where heterozygous LKB1 cooperates with KRAS mutation to the development and progression

of tumors.⁵⁷⁻⁶⁰ LKB1 activates members of AMP kinase family (AMPK) which in turn, phosphorylate effectors to repress anabolic and stimulate catabolic processes, thereby re-establishing energy homeostasis to overcome energetic stress. AMPK represses lipogenesis by inhibiting sterol regulatory element-binding transcription factor 1c (SREBP1c) and acetyl-coenzyme A (CoA) carboxylase (ACC) and impairs cholesterol synthesis by inactivating hydroxymethylglutaryl-CoA reductase,⁶¹⁻⁶³ while preventing oxidative stress secondary to defective mitochondria accumulation via ULK1-mediated mitophagy.⁶⁴ The idea of inducing a “metabolic catastrophe” to attack LKB1-deficient cancers has been tested with metformin,⁶⁵ phenformin⁴⁷ and BAY87-2243.²⁶ However, the poly-pharmacology of these compounds makes it hard to draw firm conclusions about how beneficial different aspects of metabolic catastrophe can be exploited to fight cancer. For example, LKB1-independent AMPK activation has been reported for metformin,⁶⁶ which could offer more flexibility to cancer cells to circumvent MC1 inhibition-mediated metabolic catastrophe. In this study, we show that EVT-701 did not modulate AMPK signaling in LKB1-deficient H460 cells and could inhibit tumor growth as a single agent *in vivo*. Our findings therefore point to EVT-701 as a valuable tool to explore the metabolic catastrophe approach, particularly in combination with other therapeutic approaches. We reported partial activation of MLK2 in the kinase screen. This kinase is part of the first subgroup of the Mixed Lineage Kinase family of serine/threonine protein kinases (MLK1-MLK4, sharing high sequence identity) that regulate signaling via JNK and MAPKs.⁶⁷ MLKs role in disease has essentially been described in neurodegeneration, and the potential role of MLK2 in promotion of proliferation and decrease of sensitivity to gemcitabine of pancreatic cancer was also reported.⁶⁸ Nevertheless, we do not expect this to be relevant for EVT-701 mechanism of action, since the circulating EVT-701 doses would need to be sustainably higher than 10 μ M to potentially modulate MLK2, which was not the case in *in vivo* studies presented here. EVT-701-mediated HIF-1 α degradation could be both MC1-dependent and independent. Indeed, it's been reported that Manassantin A, the natural compound from which EVT-701 was derived from Ref. [37], directly interacts with filamin A, preventing its hypoxia-induced cleavage by calpain, and stabilizing its interaction with HIF-1 α , eventually preventing its nuclear translocation and favoring its degradation.⁶⁹

In summary, EVT-701 is a novel, highly potent and selective MC1 inhibitor with an original chemical scaffold. Preclinical validation has shown *in vitro* and *in vivo* efficacy on models of NSCLC and NH B-cell lymphomas. EVT-701 is well distributed in mouse and

accumulated in several tissues compared to blood, which supports its use in a range of indications. Importantly, EVT-701 presents a safer profile than previous compounds specifically designed to inhibit MC1 and to induce HIF-1 α degradation. However, EVT-701

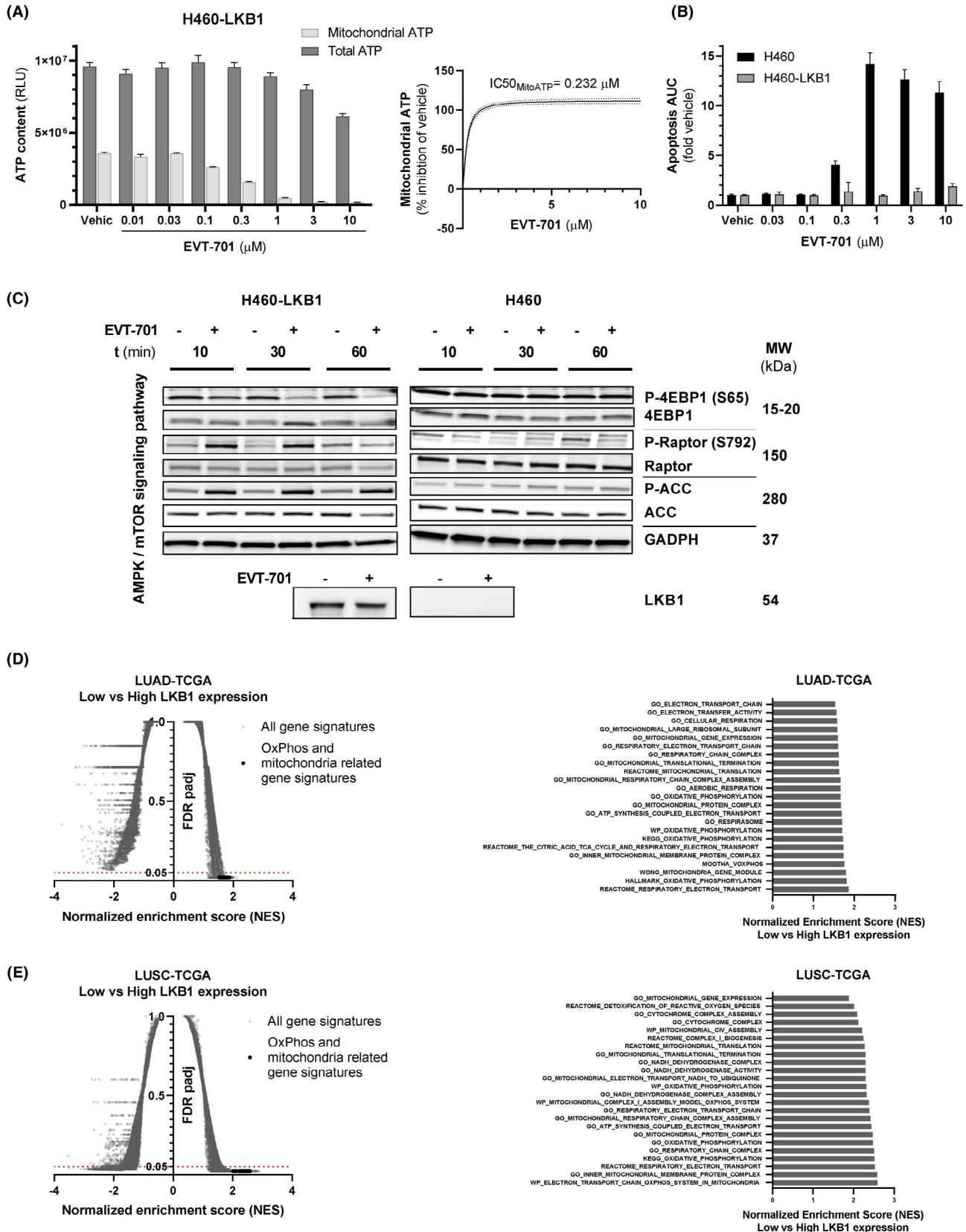


FIGURE 4 LKB1 expression as stratification marker. Exploring possible target patient populations responsive to EVT-701 treatment. The importance of LKB1 expression status on sensitivity to EVT-701. (A) Dose-dependent inhibition of mitochondrial ATP in LKB1-proficient H460 cells, with IC_{50} of 230 nM. Under the same conditions, total ATP remains unchanged whatever the dose of EVT-701. (B) Comparison of the dose-dependent induction of apoptosis by EVT-701 between LKB1-proficient H460 and WT H460 cells. Absence of LKB1 expression sensitizes H460 cells to EVT-701-induced death. (C) Modulation of mTOR/AMPK pathway signaling by EVT-701 in LKB1-proficient H460 (left) or H460 WT (right) cells over 60 min. In LKB1-proficient H460 cells (left), 4E-BP1 and Raptor phosphorylation is increased by EVT-701 treatment whereas ACC phosphorylation is inhibited. However, in WT H460 cells (right) 4E-BP1, Raptor and ACC phosphorylation are unaffected by EVT-701 at any time point. (D) Left: volcano plot showing the signatures enriched in the low versus high LKB1 expression group in The Cancer Genome Atlas Lung Adenocarcinoma (TCGA-LUAD) cohort. The enriched OxPhos and mitochondrial gene sets are highlighted in black. Right: a plot showing differentially expressed gene sets in TCGA-LUAD low LKB1 expression group (FDR <0.05) highlighted in the volcano plot with their normalized enrichment score (NES). (E) Left: volcano plot showing the signatures enriched in the low versus high LKB1 expression group in The Cancer Genome Atlas Lung Squamous Cell Carcinoma (TCGA-LUSC) cohort. The enriched OxPhos and mitochondrial gene sets are highlighted in black. Right: a plot showing differentially expressed gene sets in TCGA-LUSC low LKB1 expression group (FDR <0.05) highlighted in the volcano plot with their normalized enrichment score (NES)

shows dose-dependent interaction with efflux pumps, which impairs its accumulation overtime when dosed chronically in QD regimen. Short-term treatments of tumors presenting *de novo* or acquired sensitivity to inhibition of respiration, and therefore vulnerable to induced metabolic catastrophe, would be preferred options. LKB1 deficiency, through mutation or low expression levels, increases the sensitivity of NSCLC to EVT-701, probably due to the inability of such tumor cells to manage metabolic stress. OxPhos Non-Hodgkin's B-cell lymphomas, expressing low levels of GAPDH, are also highly susceptible to EVT-701. Patients with tumors of the aforementioned types may benefit from EVT-701 treatment. Another approach would be to combine with therapies that induce metabolic switch towards oxidative phosphorylation and so susceptibility to MC1 inhibition. EGFR inhibitor-resistant NSCLC could be a potential indication⁷⁰ as well as acute myeloid leukemia treated with cytarabine-containing regimens.¹² Altogether, these results support further investigations of EVT-701 in additional preclinical models and, eventually, in patients.

DISCLOSURE

Luna Yolba, Visentin, Hervé, Méneyrol, Paillasse and Alet and full time employees of Evotec. Chiche and Ricci declare no financial conflict of interest.

AUTHOR CONTRIBUTION

Visentin, Hervé, Chiche, Ricci, Paillasse, and Alet participated in research design. Luna Yolba, Visentin, Hervé, Chiche and Alet conducted experiments. Méneyrol contributed new reagents and analytic tools. Luna Yolba, Visentin, Hervé, Chiche, Ricci, Paillasse, and Alet performed data analysis. Luna Yolba and Paillasse wrote or contributed to the writing of the manuscript.

DATA AVAILABILITY STATEMENT

All the results and supporting data of this study are present in the manuscript and supplementary information. Upon a reasonable request, further details can be obtained from the corresponding author.

ORCID

Michaël R. Paillasse  <https://orcid.org/0000-0001-6418-8303>

REFERENCES

1. Monti S, Savage KJ, Kutok JL, et al. Molecular profiling of diffuse large B-cell lymphoma identifies robust subtypes including one characterized by host inflammatory response. *Blood*. 2005;105(5):1851-1861. <https://doi.org/10.1182/blood-2004-07-2947>
2. Weinberg F, Hamanaka R, Wheaton WW, et al. Mitochondrial metabolism and ROS generation are essential for Kras-mediated tumorigenicity. *Proc Natl Acad Sci U S A*. 2010;107(19):8788-8793. <https://doi.org/10.1073/pnas.1003428107>
3. Guo JY, Chen H-Y, Mathew R, et al. Activated Ras requires autophagy to maintain oxidative metabolism and tumorigenesis. *Genes Dev*. 2011;25(5):460-470. <https://doi.org/10.1101/gad.2016311>
4. Hensley C, Faubert B, Yuan Q, et al. Metabolic heterogeneity in human lung tumors. *Cell*. 2016;164(4):681-694. <https://doi.org/10.1016/j.cell.2015.12.034>
5. Ždravčević M, Brand A, Di Ianni L, et al. Double genetic disruption of lactate dehydrogenases A and B is required to ablate the "Warburg effect" restricting tumor growth to oxidative metabolism. *J Biol Chem*. 2018;293(41):15947-15961. <https://doi.org/10.1074/jbc.RA118.004180>
6. Momcilovic M, Shackelford DB. Targeting LKB1 in cancer-exposing and exploiting vulnerabilities. *Br J Cancer*. 2015;113(4):574-584. <https://doi.org/10.1038/bjc.2015.261>
7. Maher EA, Marin-Valencia I, Bachoo RM, et al. Metabolism of [$U-^{13}C$]glucose in human brain tumors in vivo. *NMR Biomed*. 2012;25(11):1234-1244. <https://doi.org/10.1002/nbm.2794>
8. Ju YS, Alexandrov LB, Gerstung M, et al. Origins and functional consequences of somatic mitochondrial DNA mutations in human cancer. *elife*. 2014;3:1-28. <https://doi.org/10.7554/eLife.02935>
9. Reznik ED, Miller ML, Şenbabaoğlu Y, et al. Mitochondrial DNA copy number variation across human cancers. *elife*. 2016;5:1-20. <https://doi.org/10.7554/eLife.10769>
10. Joshi S, Tolkunov D, Aviv H, et al. The genomic landscape of renal oncocytoma identifies a metabolic barrier to tumorigenesis. *Cell Rep*. 2015;13(9):1895-1908. <https://doi.org/10.1016/j.celrep.2015.10.059>
11. Faubert B, Solmonson A, DeBerardinis RJ. Metabolic reprogramming and cancer progression. *Science*. 2020;368(6487): <https://doi.org/10.1126/science.aaw5473>
12. Farge T, Saland E, de Toni F, et al. Chemotherapy-resistant human acute myeloid leukemia cells are not enriched for leukemic stem cells but require oxidative metabolism. *Cancer Discov*. 2017;7(7):716-735. <https://doi.org/10.1158/2159-8290.CD-16-0441>
13. Zickermann V, Wirth C, Nasiri H, et al. Mechanistic insight from the crystal structure of mitochondrial complex I. *Science*. 2015;347(6217):44-49. <https://doi.org/10.1126/science.1259859>
14. Brand MD, Nicholls DG. Assessing mitochondrial dysfunction in cells. *Biochem J*. 2011;435(2):297-312. <https://doi.org/10.1042/BJ20110162>

15. Fiedorczuk K, Letts JA, Degliesposti G, Kaszuba K, Skehel M, Sazanov LA. Atomic structure of the entire mammalian mitochondrial complex I. *Nature*. 2016;538(7625):406-410. <https://doi.org/10.1038/nature19794>
16. Zhu J, Vinothkumar KR, Hirst J. Structure of mammalian respiratory complex I. *Nature*. 2016;536(7616):354-358. <https://doi.org/10.1038/nature19095>
17. Rumsey WL, Schlosser C, Nuutinen EM, Robiolio M, Wilson DF. Cellular energetics and the oxygen dependence of respiration in cardiac myocytes isolated from adult rat. *J Biol Chem*. 1990;265(26):15392-15399. [https://doi.org/10.1016/S0021-9258\(18\)55409-0](https://doi.org/10.1016/S0021-9258(18)55409-0)
18. Le A, Stine ZE, Nguyen C, et al. Tumorigenicity of hypoxic respiring cancer cells revealed by a hypoxia-cell cycle dual reporter. *Proc Natl Acad Sci U S A*. 2014;111(34):12486-12491. <https://doi.org/10.1073/pnas.1402012111>
19. Jain RK, Munn LL, Fukumura D. Dissecting tumour pathophysiology using intravital microscopy. *Nat Rev Cancer*. 2002;2(4):266-276. <https://doi.org/10.1038/nrc778>
20. Masoud R, Reyes-Castellanos G, Lac S, et al. Targeting mitochondrial complex I overcomes chemoresistance in high OXPHOS pancreatic cancer. *Cell Rep Med*. 2020;1(8): 100143. <https://doi.org/10.1016/j.xcrm.2020.100143>
21. Rai N, Mathur S, Singh S, et al. Differential regulation of mitochondrial complex I and oxidative stress based on metastatic potential of colorectal cancer cells. *Oncol Lett*. 2020;20(6):1-14. <https://doi.org/10.3892/OL.2020.12176>
22. Morales DR, Morris AD. Metformin in cancer treatment and prevention. *Annu Rev Med*. 2015;66(1):17-29. <https://doi.org/10.1146/annurev-med-062613-093128>
23. Bost F, Decoux-Poullot A-G, Tanti JF, Clavel S. Energy disruptors: rising stars in anticancer therapy? *Oncogenesis*. 2016;5(1):e188. <https://doi.org/10.1038/oncsis.2015.46>
24. Zhou X, Chen J, Yi G, et al. Metformin suppresses hypoxia-induced stabilization of HIF-1 α through reprogramming of oxygen metabolism in hepatocellular carcinoma. *Oncotarget*. 2016;7(1):873-884. <https://doi.org/10.18632/oncotarget.6418>
25. Griss T, Vincent EE, Egnatchik R, et al. Metformin antagonizes cancer cell proliferation by suppressing mitochondrial-dependent biosynthesis. *PLoS Biol*. 2015;13(12):1-23. <https://doi.org/10.1371/journal.pbio.1002309>
26. Ellinghaus P, Heisler I, Unterschemmann K, et al. BAY 87-2243, a highly potent and selective inhibitor of hypoxia-induced gene activation has antitumor activities by inhibition of mitochondrial complex I. *Cancer Med*. 2013;2(5):611-624. <https://doi.org/10.1002/cam4.112>
27. Schöckel L, Glasauer A, Basit F, et al. Targeting mitochondrial complex I using BAY 87-2243 reduces melanoma tumor growth. *Cancer Metab*. 2015;3(1):1-16. <https://doi.org/10.1186/s40170-015-0138-0>
28. Molina JR, Sun Y, Protopopova M, et al. An inhibitor of oxidative phosphorylation exploits cancer vulnerability. *Nat Med*. 2018;24(7):1036-1046. <https://doi.org/10.1038/s41591-018-0052-4>
29. Yap TA, Rodon Ahnert J, Piha-Paul SA, et al. Phase I trial of IACS-010759 (IACS), a potent, selective inhibitor of complex I of the mitochondrial electron transport chain, in patients (pts) with advanced solid tumors. *J Clin Oncol*. 2019;37(15_suppl):3014. https://doi.org/10.1200/JCO.2019.37.15_suppl.3014
30. Chiche J, Pommier S, Beneteau M, et al. GAPDH enhances the aggressiveness and the vascularization of Non-Hodgkin's B lymphomas via NF- κ B-dependent induction of HIF-1 α . *Leukemia*. 2015;29(5):1163-1176. <https://doi.org/10.1038/leu.2014.324>
31. Chiche J, Reverso-Meinietti J, Mouchotte A, et al. GAPDH expression predicts the response to R-CHOP, the tumor metabolic status, and the response of DLBCL patients to metabolic inhibitors. *Cell Metab*. 2019;29(6):1243-1257.e10. <https://doi.org/10.1016/j.cmet.2019.02.002>
32. Sabri MI, Ochs S. Inhibition of glyceraldehyde-3-phosphate dehydrogenase in mammalian nerve by iodoacetic acid. *J Neurochem*. Published online. 1971;18(8):1509-1514. <https://doi.org/10.1111/j.1471-4159.1971.tb00013.x>
33. Schmidt MM. Differential effects of iodoacetamide and iodoacetate on glycolysis and glutathione metabolism of cultured astrocytes. *Front Neuroenergetics*. 2009;1:1. <https://doi.org/10.3389/neuro.14.001.2009>
34. Harding SD, Sharman JL, Faccenda E, et al. The IUPHAR/BPS Guide to PHARMACOLOGY in 2018: updates and expansion to encompass the new guide to IMMUNOPHARMACOLOGY. *Nucleic Acids Res*. 2018;46:D1091-D1106. <https://doi.org/10.1093/nar/gkx1121>
35. Alexander SPH, Kelly E, Mathie A, et al. THE CONCISE GUIDE TO PHARMACOLOGY 2019/20: introduction and other protein targets. *Br J Pharmacol*. 2019; 176:S1-S20. <https://doi.org/10.1111/bph.14747>
36. Alexander SPH, Fabbro D, Kelly E, et al. THE CONCISE GUIDE TO PHARMACOLOGY 2019/20: enzymes. *Br J Pharmacol*. 2019;176(S1):S297-S396. <https://doi.org/10.1111/bph.14752>
37. Méneyrol J, Alet N, Barre G, Rousseaux T, Vin V. Benzylhydroxide derivatives, preparation thereof and therapeutic use thereof. 2016. <https://register.epo.org/application?number=EP15788381&stab=main>
38. Gao ZY, Liu Z, Bi MH, et al. Metformin induces apoptosis via a mitochondria-mediated pathway in human breast cancer cells in vitro. *Exp Ther Med*. 2016;11(5):1700-1706. <https://doi.org/10.3892/etm.2016.3143>
39. Gao X, Qiao X, Xing X, et al. Matrix stiffness-upregulated microRNA-17-5p attenuates the intervention effects of metformin on HCC invasion and metastasis by targeting the PTEN/PI3K/Akt pathway. *Front Oncol*. 2020;10:1-13. <https://doi.org/10.3389/fonc.2020.01563>
40. Sesen J, Dahan P, Scotland SJ, et al. Metformin inhibits growth of human glioblastoma cells and enhances therapeutic response. *PLoS One*. 2015;10(4):1-24. <https://doi.org/10.1371/journal.pone.0123721>
41. Patricelli M, Nomanbhoy T, Wu J, et al. In situ kinase profiling reveals functionally relevant properties of native kinases. *Chem Biol*. 2011;18(6):699-710. <https://doi.org/10.1016/j.chembiol.2011.04.011>
42. Ricci JE, Chiche J. Metabolic reprogramming of Non-Hodgkin's B-cell lymphomas and potential therapeutic strategies. *Front Oncol*. 2018;8:1-23. <https://doi.org/10.3389/fonc.2018.00556>
43. Caro P, Kishan A, Norberg E, et al. Metabolic signatures uncover distinct targets in molecular subsets of diffuse large B cell lymphoma. *Cancer Cell*. 2012;22(4):547-560. <https://doi.org/10.1016/j.ccr.2012.08.014>
44. Adams JM, Harris AW, Pinkert CA, et al. The c-myc oncogene driven by immunoglobulin enhancers induces lymphoid malignancy in transgenic mice. *Nature*. 1985;318(6046):533-538. <https://doi.org/10.1038/318533a0>
45. Chuang MC, Yang YH, Tsai YH, et al. Survival benefit associated with metformin use in inoperable non-small cell lung cancer patients with diabetes: a population-based retrospective cohort study. *PLoS One*. 2018;13(1):1-11. <https://doi.org/10.1371/journal.pone.0191129>
46. Doki Y, Murakami K, Yamaura T, Sugiyama S, Misaki T, Saiki I. Mediastinal lymph node metastasis model by orthotopic intrapulmonary implantation of Lewis lung carcinoma cells in mice. *Br J Cancer*. 1999;79(7-8):1121-1126. <https://doi.org/10.1038/sj.bjc.6690178>
47. Shackelford D, Abt E, Gerken L, et al. LKB1 inactivation dictates therapeutic response of non-small cell lung cancer to the metabolism drug phenformin. *Cancer Cell*. 2013;23(2):143-158. <https://doi.org/10.1016/j.ccr.2012.12.008>
48. Raes F, Sobilo J, Le Mée M, et al. High resolution ultrasound and photoacoustic imaging of orthotopic lung cancer in mice: new

- perspectives for onco-pharmacology. *PLoS One*. 2016;11(4):1-15. <https://doi.org/10.1371/journal.pone.0153532>
49. Faubert B, Vincent EE, Griss T, et al. Loss of the tumor suppressor LKB1 promotes metabolic reprogramming of cancer cells via HIF-1 α . *Proc Natl Acad Sci U S A*. 2014;111(7):2554-2559. <https://doi.org/10.1073/pnas.1312570111>
 50. Kaufman JM, Amann JM, Park K, et al. LKB1 loss induces characteristic patterns of gene expression in human tumors associated with NRF2 activation and attenuation of PI3K-AKT. *J Thorac Oncol*. 2014;9(6):794-804. <https://doi.org/10.1097/JTO.0000000000000173>
 51. Whang YM, Park SI, Trenary IA, et al. LKB1 deficiency enhances sensitivity to energetic stress induced by erlotinib treatment in non-small-cell lung cancer (NSCLC) cells. *Oncogene*. 2016;35(7):856-866. <https://doi.org/10.1038/onc.2015.140>
 52. Zhang Y, Meng Q, Sun Q, Xu ZX, Zhou H, Wang Y. LKB1 deficiency-induced metabolic reprogramming in tumorigenesis and non-neoplastic diseases. *Mol Metab*. 2021;44:101131. <https://doi.org/10.1016/j.molmet.2020.101131>
 53. Borzi C, Galli G, Ganzinelli M, et al. Beyond lkb1 mutations in non-small cell lung cancer: defining lkb1less phenotype to optimize patient selection and treatment. *Pharmaceuticals*. 2020;13(11):1-12. <https://doi.org/10.3390/ph13110385>
 54. Korse SE, Peppelenbosch MP, Van Veelen W. Targeting LKB1 signaling in cancer. *Biochim Biophys Acta - Rev Cancer*. 2013;1835(2):194-210. <https://doi.org/10.1016/j.bbcan.2012.12.006>
 55. Jenne DE, Reomann H, Nezu J, et al. Peutz-Jeghers syndrome is caused by mutations in a novel serine threonine kinase. *Nat Genet*. 1998;18(1):38-43. <https://doi.org/10.1038/ng0198-38>
 56. Giardiello FM, Welsh SB, Hamilton SR, et al. Increased risk of cancer in the Peutz-Jeghers syndrome. *N Engl J Med*. 1987;316(24):1511-1514. <https://doi.org/10.1056/NEJM198706113162404>
 57. Hollstein PE, Eichner LJ, Brun SN, et al. The AMPK-related kinases SIK1 and SIK3 mediate key tumor-suppressive effects of LKB1 in NSCLC. *Cancer Discov*. 2019;9(11):1606-1627. <https://doi.org/10.1158/2159-8290.CD-18-1261>
 58. Galan-Cobo A, Sitthideatphaiboon P, Qu X, et al. LKB1 and KEAP1/NRF2 pathways cooperatively promote metabolic reprogramming with enhanced glutamine dependence in KRAS-mutant lung adenocarcinoma. *Cancer Res*. 2019;79(13):3251-3267. <https://doi.org/10.1158/0008-5472.CAN-18-3527>
 59. Sanchez-Vega F, Mina M, Armenia J, et al. Oncogenic signaling pathways in The Cancer Genome Atlas. *Cell*. 2018;173(2):321-337. <https://doi.org/10.1016/j.cell.2018.03.035>
 60. Morton JP, Jamieson NB, Karim SA, et al. LKB1 haploinsufficiency cooperates with Kras to promote pancreatic cancer through suppression of p21-dependent growth arrest. *Gastroenterology*. 2010;139(2):586-597. <https://doi.org/10.1053/j.gastro.2010.04.055>
 61. Li YU, Xu S, Mihaylova MM, et al. AMPK phosphorylates and inhibits SREBP activity to attenuate hepatic steatosis and atherosclerosis in diet-induced insulin-resistant mice. *Cell Metab*. 2011;13(4):376-388. <https://doi.org/10.1016/j.cmet.2011.03.009>
 62. Munday MR, Carling D, Hardie DG. Negative interactions between phosphorylation of acetyl-CoA carboxylase by the cyclic AMP-dependent and AMP-activated protein kinases. *FEBS Lett*. 1988;235(1-2):144-148. [https://doi.org/10.1016/0014-5793\(88\)81251-1](https://doi.org/10.1016/0014-5793(88)81251-1)
 63. Vara-Ciruelos D, Russell FM, Hardie DG. The strange case of AMPK and cancer: Dr Jekyll or Mr Hyde? *Open Biol*. 2019;9(7):190099. <https://doi.org/10.1098/rsob.190099>
 64. Egan DF, Shackelford DB, Mihaylova MM, et al. Phosphorylation of ULK1 (hATG1) by AMP-activated protein kinase connects energy sensing to mitophagy. *Science*. 2011;331(6016):456-461. <https://doi.org/10.1126/science.1196371>
 65. Moro M, Caiola E, Ganzinelli M, et al. Metformin enhances cisplatin-induced apoptosis and prevents resistance to cisplatin in co-mutated KRAS/LKB1 NSCLC. *J Thorac Oncol*. 2018;13(11):1692-1704. <https://doi.org/10.1016/j.jtho.2018.07.102>
 66. Guo Q, Liu Z, Jiang L, et al. Metformin inhibits growth of human non-small cell lung cancer cells via liver kinase B-1-independent activation of adenosine monophosphate-activated protein kinase. *Mol Med Rep*. 2016;13(3):2590-2596. <https://doi.org/10.3892/mmr.2016.4830>
 67. Kashuba VI, Grigorieva EV, Kvasha SM, et al. Cloning and initial functional characterization of Mlk4a and Mlk4b. *Genomics Insights*. 2011;4(1):1-12. <https://doi.org/10.4137/GEI.S6092>
 68. An Y, Cai B, Chen J, et al. MAP3K10 promotes the proliferation and decreases the sensitivity of pancreatic cancer cells to gemcitabine by upregulating Gli-1 and Gli-2. *Cancer Lett*. 2013;329(2):228-235. <https://doi.org/10.1016/j.canlet.2012.11.005>
 69. Geer Wallace MA, Kwon D-Y, Weitzel DH, et al. Discovery of manassantin A protein targets using large-scale protein folding and stability measurements. *J Proteome Res*. 2016;15(8):2688-2696. <https://doi.org/10.1021/acs.jproteome.6b00237>
 70. De Rosa V, Iommelli F, Monti M, et al. Reversal of warburg effect and reactivation of oxidative phosphorylation by differential inhibition of EGFR signaling pathways in non-small cell lung cancer. *Clin Cancer Res*. 2015;21(22):5110-5120. <https://doi.org/10.1158/1078-0432.CCR-15-0375>

SUPPORTING INFORMATION

Additional supporting information may be found online in the Supporting Information section.

How to cite this article: Luna Yolba R, Visentin V, Hervé C, et al. EVT-701 is a novel selective and safe mitochondrial complex 1 inhibitor with potent anti-tumor activity in models of solid cancers. *Pharmacol Res Perspect*. 2021;9:e00854. <https://doi.org/10.1002/prp2.854>